WMO Statement on the Status of the Global Climate in 2015

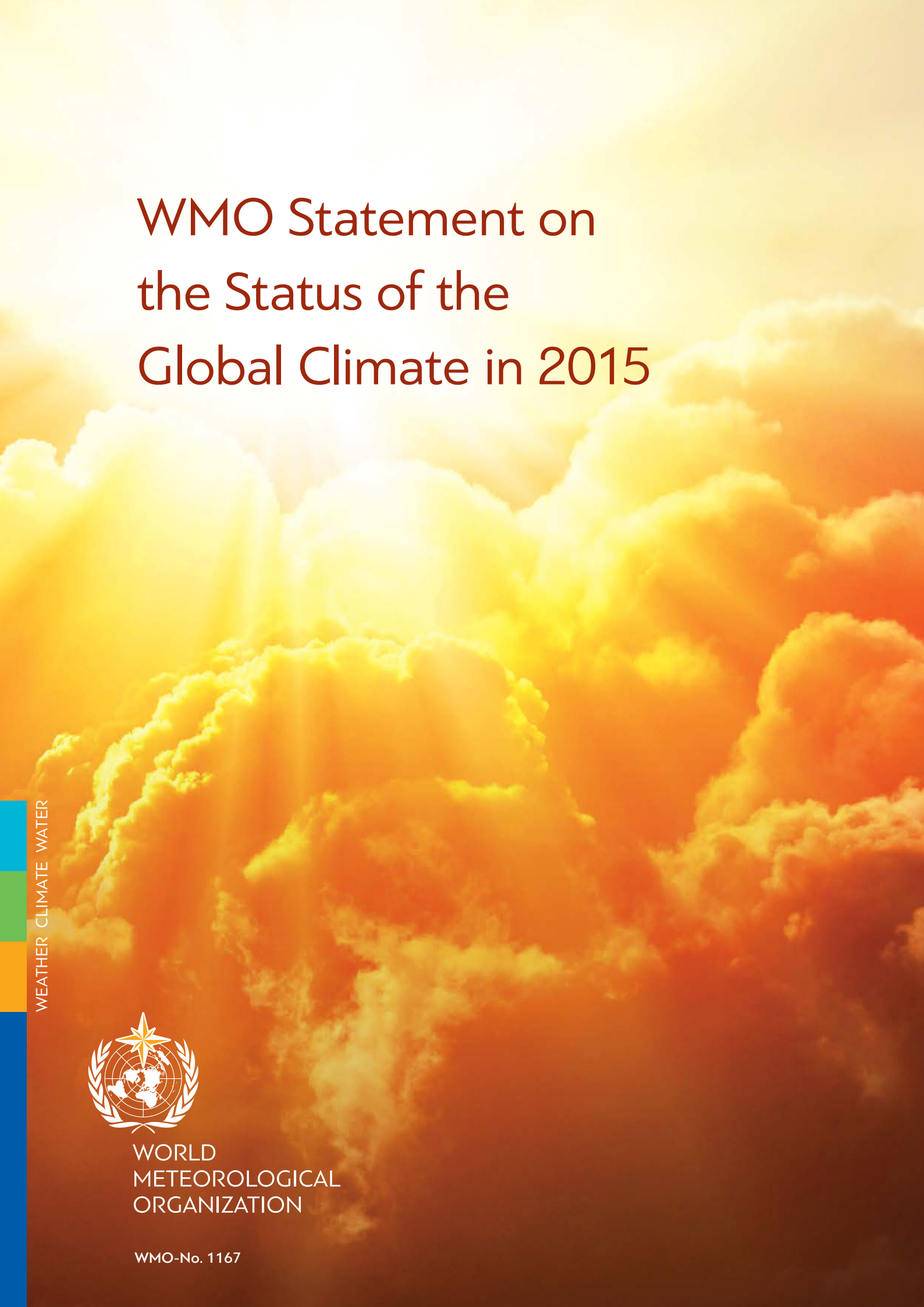

WEATHER CLIMATE WATER

WORLD METEOROLOGICAL ORGANIZATION

WMO-No. 1167

WMO-No. 1167

Chairperson, Publications Board
World Meteorological Organization (WMO)
7 bis, avenue de la Paix
P.O. Box 2300
CH-1211 Geneva 2, Switzerland

Tel.: +41 (0) 22 730 84 03
Fax: +41 (0) 22 730 80 40
E-mail: publications@wmo.int

ISBN 978-92-63-11167-8

WMO, in collaboration with Members, began issuing annual statements on the status of the global climate in 1993. This publication was issued in collaboration with the African Centre of Meteorological Applications for Development (ACMAD), Niger; European Centre for Medium-Range Weather Forecasts (ECMWF), United Kingdom of Great Britain and Northern Ireland; Japan Meteorological Agency (JMA); Met Office Hadley Centre, United Kingdom; Climatic Research Unit (CRU) at the University of East Anglia, United Kingdom; Climate Prediction Center (CPC), the National Centers for Environmental Information (NCEI) and the National Hurricane Center (NHC) of the National Oceanic and Atmospheric Administration (NOAA), United States of America; National Aeronautics and Space Administration, Goddard Institute for Space Studies (NASA GISS), United States; Global Precipitation Climatology Centre (GPCC), Germany; National Snow and Ice Data Center (NSIDC), United States; Commonwealth Scientific and Industrial Research Organization (CSIRO) Marine and Atmospheric Research, Australia; Global Snow Lab, Rutgers University, United States; International Research Centre on El Niño (CIIFEN), Ecuador; Royal Netherlands Meteorological Institute (KNMI), Netherlands; Institute on Global Climate and Ecology (IGCE), Russian Federation; All-Russian Research Institute for Hydrometeorological Information – World Data Center (ARIHMI-WDC), Russian Federation. Other contributors are the National Meteorological and Hydrological Services or equivalent of: Argentina; Armenia; Australia; Austria; Azerbaijan; Bosnia and Herzegovina; Burkina Faso; Canada; China; Cyprus; Denmark; Estonia; Fiji; Finland; France; Germany; Hong Kong, China; Hungary; India; Indonesia; Iran, Islamic Republic of; Ireland; Israel; Japan; Jordan; Libya; Mali; Mauritius; Mexico; Montenegro; Morocco; New Zealand; Niger; Norway; Pakistan; Poland; Republic of Korea; Republic of Moldova; Russian Federation; Serbia; Slovakia; Slovenia; South Africa; Spain; Sweden; Switzerland; Thailand; Ukraine; United Kingdom; United Republic of Tanzania; and United States.

Cover illustration: Shutterstock.com

Contents

Warmest year on record by far, 0.76 °C above 1961–1990 average

2015

1°

Increase above pre-industrial era; halfway to 2 °C limit

EL NIÑO

One of the strongest on record; combined with climate change from human activities to drive global temperatures to new peak

Heatwaves, droughts, floods, strong tropical cyclones

400 ppm

CO_2 concentrations breach symbolic benchmark in northern hemisphere spring

Excess energy from greenhouse gas emissions stored in oceans; record global ocean heat content down to 2 000 m.

93%

Foreword

As part of its mandate to provide authoritative information about weather, climate and water, the World Meteorological Organization (WMO) conducts annual assessments of the state of the global climate. For over two decades, those assessments have been published in the six official languages of the United Nations in order to inform governments, international agencies and other WMO partners about global climate trends, and extreme and notable weather and climate events at the national and regional levels.

The year 2015 will stand out in the historical record of the global climate in many ways. Modern records for heat were broken: 2015 was a record warm year both globally and in many individual countries. Heatwaves were extremely intense in various part of the world, leading to thousands of deaths in India and Pakistan. Record extreme precipitation led to flooding that affected tens of thousands of people across South America, West Africa and Europe. Dry conditions in southern Africa and Brazil exacerbated multi-year droughts. The influence of the strong El Niño that developed in the later part of 2015 can be discerned in many of the year's weather and climate events. While much work remains to be done, advances in international collaboration, the near-real-time sharing of data, and progress in attribution science are starting to make it possible to disentangle the respective roles played by El Niño, other natural climate variations and human-induced climate change.

On a more positive note, the Parties to the United Nations Framework Convention on Climate Change adopted the groundbreaking Paris Agreement in December. The world's governments unanimously agreed to take action in order to reduce global emissions of greenhouse gases into the atmosphere. They will aim to hold the increase in the global average temperature to well below 2 °C above pre-industrial levels and to pursue efforts to limit the temperature increase to 1.5 °C. The Paris Agreement raises hope that international efforts to safeguard our planet will be accelerated in order to avoid reaching a point of no return for the climate system. However, the warming trend and an increasing number of disasters are expected to continue for several decades. That emphasizes the need to invest in adaptation as well as mitigation. One of the most powerful ways to adapt to the consequences of climate change is to strengthen disaster early warning and climate services.

WMO is committed to further enhancing weather and climate services and related research. But in addition to promoting scientific progress, WMO recognizes the need to build operational climate services that support climate resilience and adaptation. Some 70 countries around the world do not have the capabilities they need to generate and apply climate information and forecasts with the required timeliness and quality of service. The Global Framework for Climate Services is assisting least developed countries, small island developing States and other vulnerable countries to strengthen their national climate and meteorological capabilities. WMO is also working with its partners to help countries protect themselves from climate risks through multi-hazard early warning systems, impact-based forecasts and risk-informed warnings.

I would like to take this opportunity to express my gratitude to the National Meteorological and Hydrological Services of the WMO Members, to international and regional data centres and institutions, and to climate experts from around the world: they have all contributed to developing this annual statement according to the highest scientific standards.

WMO welcomes suggestions from its Members on how to further improve the Statement on the Status of the Global Climate, including in light of new requirements arising from the Paris Agreement, the Sendai Framework for Disaster Risk Reduction 2015–2030, and the United Nations Sustainable Development Goals.

(P. Taalas)
Secretary-General

Introduction

The *WMO Statement on the Status of the Global Climate in 2015* covers many aspects of the climate system, including atmospheric and ocean conditions, El Niño, the cryosphere, greenhouse gas concentrations, regional extremes, tropical cyclones and ozone depletion. The Statement draws on in situ and space-based observations collected through various WMO and co-sponsored programmes. It also draws on numerical objective analyses. These observations are the Essential Climate Variables that have been defined by the Global Climate Observing System.

The international datasets underpinning this assessment are maintained by advanced climate data, monitoring and research centres that collaborate with WMO. In addition, data and climate information has been collected directly from WMO Members through a special WMO survey. The global temperature analysis combines three international datasets: the first (HadCRUT) is maintained by the Met Office Hadley Centre in collaboration with the Climatic Research Unit at the University of East Anglia (both in the United Kingdom of Great Britain and Northern Ireland); the second is kept by the National Oceanic and Atmospheric Administration National Centers for Environmental Information (United States of America); and the third is maintained by the National Aeronautics and Space Administration, Goddard Institute for Space Studies (United States). The WMO analysis also incorporates reanalysis data maintained by the European Centre for Medium-Range Weather Forecasts and by the Japanese Meteorological Agency. Global precipitation information is provided by the Global Precipitation Climatology Centre (Germany).

The assessment of national temperature anomalies uses data collected directly from Members through a WMO survey. Data used in this publication relating to socioeconomic impacts are based on reports provided directly by Members or are taken from authoritative United Nations sources. The peer-review process involves international climate experts, regional institutions dealing with climate products and experts from the National Meteorological and Hydrological Services. In some cases, it was necessary to cross-check with national focal points in order to validate or update information available from global sources.

HAWAII, UNITED STATES

A powerful El Niño combined with rising temperatures is destroying the world's coral reefs, causing the longest die-off event on record.

NOAA

Key findings

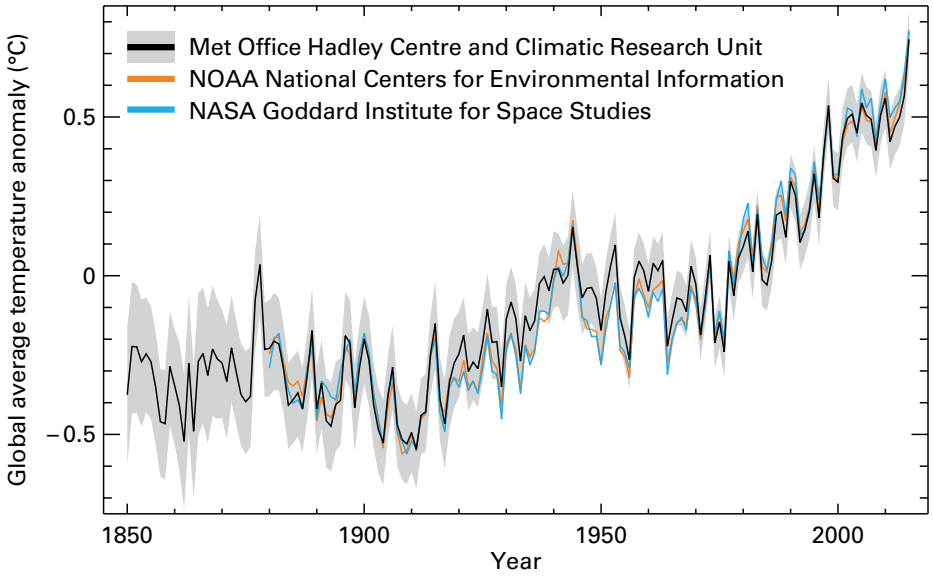

Figure 1. Global annual average temperature anomalies (relative to 1961–1990) for 1850–2015. The black line and grey shading are from the HadCRUT4 analysis produced by the Met Office Hadley Centre in collaboration with the Climatic Research Unit at the University of East Anglia. The grey shading indicates the 95% confidence interval of the estimates. The orange line is the NOAAGlobalTemp dataset produced by the National Oceanic and Atmospheric Administration National Centers for Environmental Information (NOAA NCEI). The blue line is the GISTEMP dataset produced by the National Aeronautics and Space Administration, Goddard Institute for Space Studies (NASA GISS). *(Source: Met Office Hadley Centre, United Kingdom, and Climatic Research Unit, University of East Anglia, United Kingdom)*

TEMPERATURE

In 2015, global warmth reached record levels as a result of the long-term rise in global temperatures (caused mostly by humanity's emissions of greenhouse gases) combined with the effects of a developing El Niño.

The global average near-surface temperature for 2015 was the warmest on record by a clear margin, according to data sources[1] analysed by WMO (Figure 1). The global average temperature for the year was about 0.76 ± 0.09 °C above the 1961–1990 average, and approximately 1 °C above the 1850–1900 average. Uncertainties relative to the period 1850–1900 are larger and more difficult to estimate.

These estimates are based on air-temperature data gathered at meteorological stations over land, and sea-surface temperatures measured at sea, both by ships in the voluntary observing fleet and by drifting and moored buoys. The estimates are corroborated by an analysis produced by the Japan Meteorological Agency.

Global average temperatures can also be estimated using output from reanalyses. In a reanalysis, historical observations from many different instruments are combined using a modern weather forecasting system, in order to give a comprehensive record of weather and climate. Two long-term reanalyses were surveyed: the ERA-Interim reanalysis, produced by the European Centre for Medium-Range Weather Forecasts, and the JRA-55 reanalysis, produced by the Japan Meteorological Agency. The central estimates for both of those reanalyses indicate that 2015 was the warmest year on record near the surface.

The global average of temperatures over land areas shows that 2015 was the joint warmest year on record over land: 2005, 2007 and 2010 are comparable. The global average temperature over the sea surface in 2015 was equal to the 2014 record. The combination of high land and sea temperatures made 2015 a record year overall.

Significant warmth was recorded over the majority of observed land areas (Figure 2). Particularly warm were large areas of South

[1] **HadCRUT4.4.0.0** produced by the Met Office Hadley Centre in collaboration with the Climatic Research Unit at the University of East Anglia (both in the United Kingdom); **GISTEMP** produced by the National Aeronautics and Space Administration, Goddard Institute for Space Studies (United States); and **NOAAGlobalTemp** produced by the National Oceanic and Atmospheric Administration National Centers for Environmental Information (United States). The number quoted is an average of those three datasets. Its uncertainty is taken from the HadCRUT4 dataset.

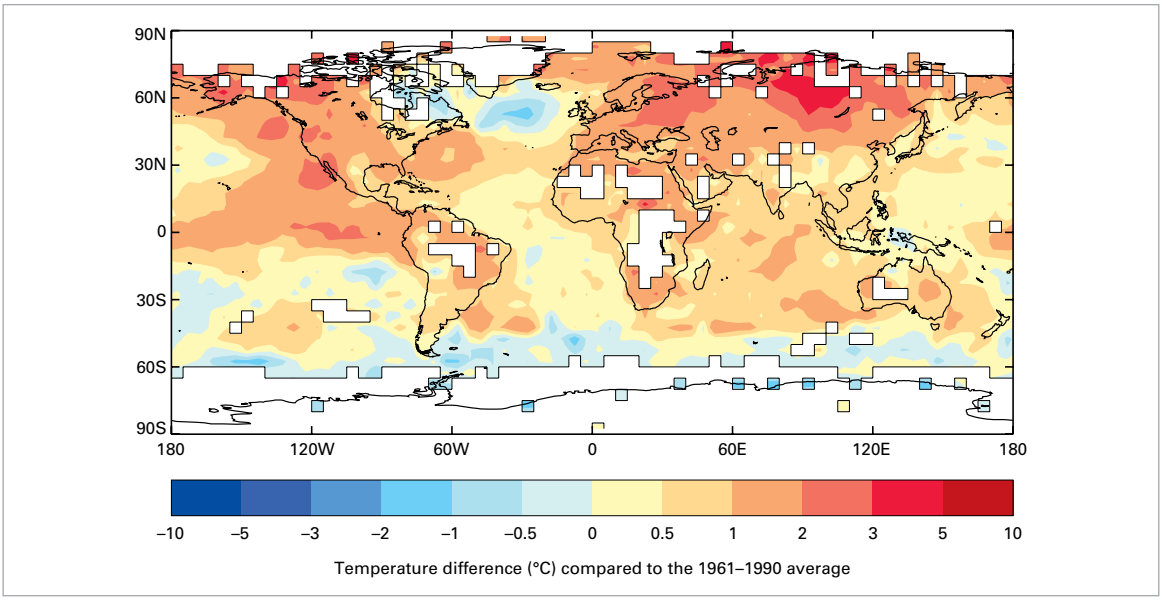

Figure 2. Annual average near-surface temperature anomalies (temperature difference from the 1961–1990 average) for 2015 from the HadCRUT4 dataset *(Source: Met Office Hadley Centre, United Kingdom)*

America, Africa, much of Europe, North-East Eurasia, the Middle East and western parts of North America. Continental temperature records were set for Asia and South America. The Russian Federation had its warmest year on record, at 2.16 °C above the 1961–1990 average. China also had its warmest year on record (since at least 1961) and 10 of its provinces experienced record warmth. Europe experienced either its second-warmest year (after 2014) or its warmest, and 2015 was either the warmest year in a number of countries (Estonia, Finland, Spain) or was one of the top three warmest years (Germany, France, Slovenia, Republic of Moldova, Hungary, Serbia). Africa and Oceania each experienced their second-warmest year on record.

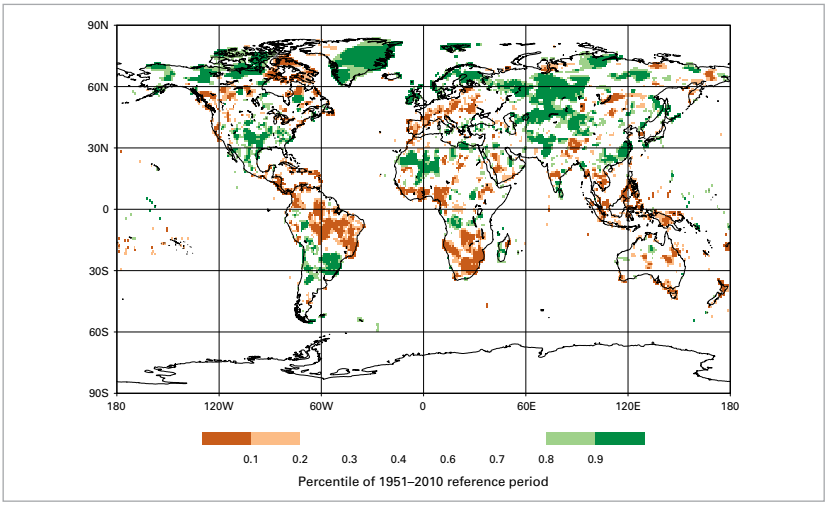

Figure 3. Annual total precipitation expressed as a percentile of the 1951–2010 reference period for areas that would have been in the driest 20% (brown) and wettest 20% (green) of years during the reference period, with darker shades of brown and green indicating the driest and wettest 10%, respectively *(Source: Global Precipitation Climatology Centre, Deutscher Wetterdienst, Germany)*

Few land areas experienced significant cold conditions when averaged over the year. One notably colder-than-average area was the Antarctic, where the positive phase of the Southern Annular Mode (SAM) persisted for several months. In the positive phase of SAM, westerly winds strengthen and contract towards Antarctica. That induces cooling over most of East Antarctica and warming over the Antarctic Peninsula. October saw a change to less extreme values of the SAM index through to the end of the year and a warming relative to average over the continent. Some north-eastern areas of North America were colder than average during the year.

PRECIPITATION AND SNOW COVER

In a typical year the distribution of precipitation is highly variable at regional and local scales; 2015 was no exception. Rainfall extremes affected many regions around the world and in some cases, led to flooding and drought. The section below on regional extremes provides more details on rainfall extremes and related impacts.

On the annual scale, there were areas of unusually high rainfall (Figure 3), including: southern areas of the United States, Mexico, Peru, northern Chile, most of the Plurinational State of Bolivia, Paraguay, southern Brazil and northern Argentina, northern and South-East

Europe, parts of Central Asia, South-East China, areas of Pakistan, and Afghanistan. On the other hand, dry areas included Central America and the Caribbean, north-east South America including Brazil, parts of central and southern Europe, parts of South-East Asia, Indonesia, and southern Africa. Although long-term accumulations are important, they can disguise great variability in short-term totals.

According to the Global Snow Lab at Rutgers University, the snow extent in the northern hemisphere during spring was 28.5 million km^2. That is below the long-term average and is the eighth-lowest on record. North America had its fourth-lowest spring snow extent on record. However, in the United States, numerous snow storms affected the North-East in February. Massachusetts, Boston and Worcester saw their all-time snowiest month and snowiest winter. In Boston, 164.6 cm of snow fell during February, which is more than normally falls in the city in an entire season.

OCEANS

Over the oceans, significant warmth was recorded across large areas. As would be expected during an El Niño, the tropical Pacific was much warmer than average and over 1 °C warmer than average over much of the central and eastern equatorial Pacific (Figure 2). The North-East Pacific, much of the Indian Ocean and areas in the North and South Atlantic were also significantly warmer. Areas to the south of Greenland and in the far South-West Atlantic were significantly colder than average. Other areas of the Southern Ocean (approximately south of 60°S) were colder than average, but in many cases there are too few data in the climatology period (1961–1990) to reliably estimate the significance of current anomalies.

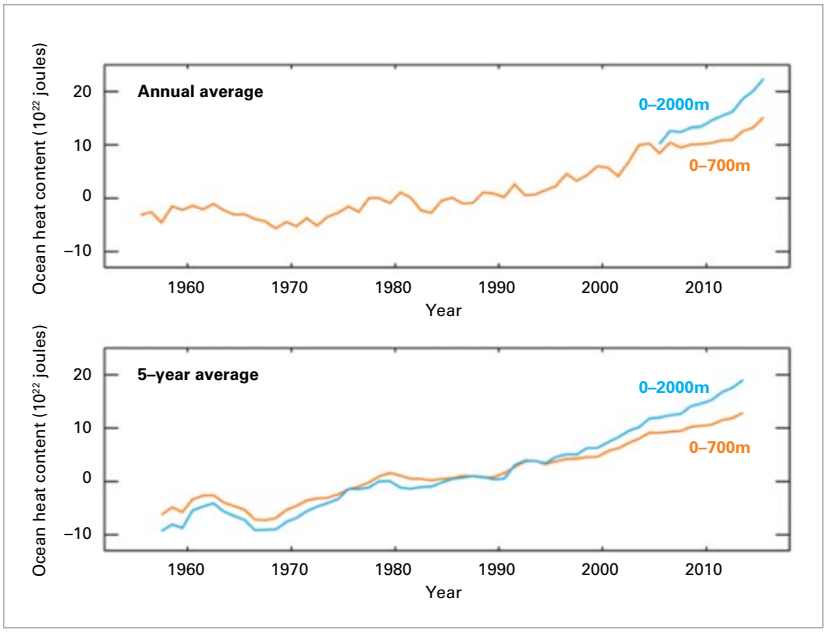

Figure 4. Annual average ocean heat content in the upper 700 m (orange) and the upper 2 000 m (blue) of the ocean (top), and five-year-average ocean heat content (bottom). Annual averages down to 2 000 m are only shown from 2005, from which time near-global coverage is provided down to 2 000 m on an annual-or-better basis by the Argo array.
(Source: Data from NOAA/NESDIS/NODC Ocean Climate Laboratory, United States, updated from Levitus et al. (2012))

In 2015, global ocean heat content reached record levels through both the upper 700 m and 2 000 m of the oceans (Figure 4). Routine measurements of temperatures down to 2 000 m are now made using Argo floats. For more details and background on ocean heat content, see page 22.

Sea level is measured by satellites as well as by traditional tide gauges. The latest estimates of the global sea level from satellite altimeters (Figure 5) indicate that the global average sea level for January to November 2015 was the highest ever recorded by satellites. In line with the long-term upward trend in sea level as estimated by tide gauges, the same period also saw the highest recorded sea level since global records began more than a century ago.

Even though the global average sea level reached record levels in 2015, not all areas of the ocean did. Monthly average sea levels were lower than normal in the western tropical Pacific, as might be expected during an El Niño. In the latter half of

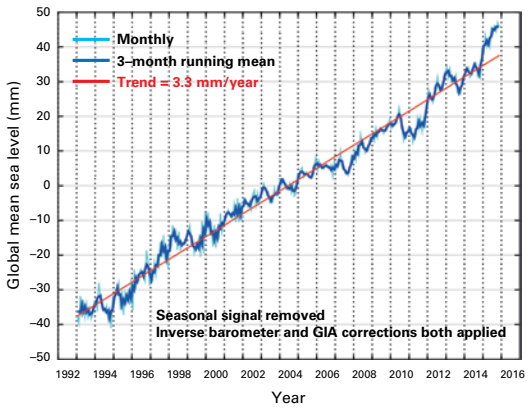

Figure 5. Global mean sea-level change 1993 to November 2015, with annual cycle removed from the data; monthly values shown in pale blue, three-month averages in dark blue and a simple linear trend in red.
(Source: Commonwealth Scientific and Industrial Research Organization, Australia)

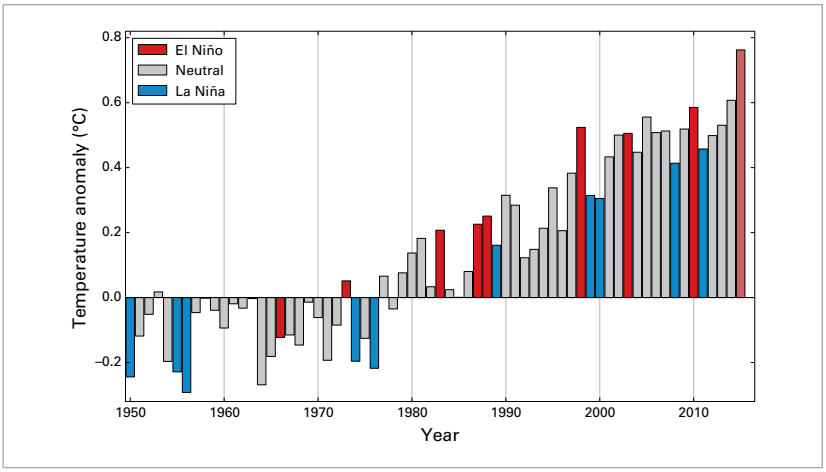

Figure 6. Global annual average temperature anomalies (difference from the 1961–1990 average) based on an average of the three global temperature datasets. Coloured bars indicate years that were influenced by El Niño (red) and La Niña (blue), and the years without a strong influence (grey). The pale red bar indicates 2015. *(Source: Met Office Hadley Centre, United Kingdom, and Climatic Research Unit, University of East Anglia, United Kingdom)*

the year, negative sea-level anomalies of about –10 cm were reported in the Marshall Islands, the Federated States of Micronesia and Papua New Guinea. The anomalies were smaller than those observed during the 1997/1998 El Niño. By contrast, sea levels along the Equator east of the dateline were above average: that is also symptomatic of an El Niño.

EL NIÑO

Variations in the temperature of the surface waters of the tropical Pacific combine with atmospheric feedbacks to drive the two distinct phases of the El Niño Southern Oscillation, El Niño and La Niña. During an El Niño, sea-surface temperatures in the eastern tropical Pacific rise above average. This leads to a weakening or reversal of the prevailing trade winds, which acts to reinforce surface warming. The El Niño Southern Oscillation is the leading mode of year-to-year global climate variability. El Niño affects the global atmospheric circulation, altering weather patterns around the world and temporarily elevating global temperatures.

In 2015, sea-surface temperatures in the East-Central Pacific increased, exceeding typical El Niño thresholds during northern hemisphere spring. Atmospheric indicators were also indicative of a developing El Niño, such as the pressure difference between Tahiti and Darwin, enhanced convection near the dateline, and a weakening or reversal of the trade winds. El Niño continued to strengthen and peaked in December. At its peak, sea-surface temperatures in some key areas were comparable to those recorded during the exceptionally strong El Niño events of 1997/1998 and 1982/1983, though the location of the peak sea-surface temperature anomalies was further to the west in 2015.

El Niño affects rainfall and weather patterns in many places around the world. Although the

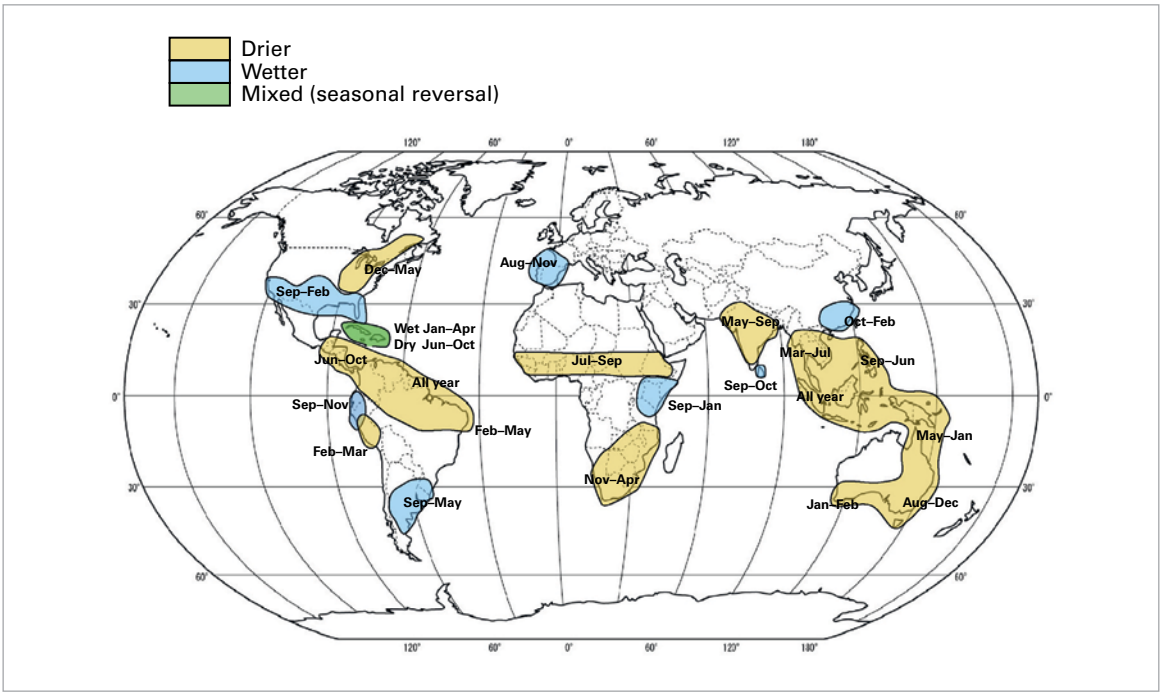

Figure 7. Precipitation anomalies favoured during El Niño, based on historical rates of occurrence during previous El Niño events *(Source: adapted from Met Office Hadley Centre, United Kingdom)*

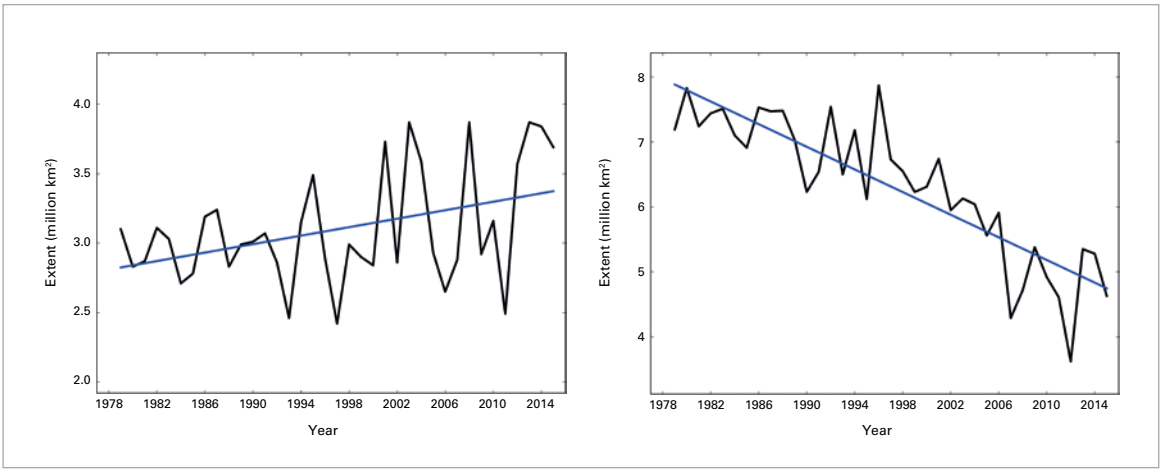

Figure 8. Monthly sea-ice extent for February in the southern hemisphere (left) and September in the northern hemisphere (right) for 1979–2015 *(Source: National Snow and Ice Data Center, NOAA, United States)*

precise details of any single El Niño will differ, certain recurrent patterns might be expected during a strong El Niño.

El Niño is typically associated with higher global temperatures both at the surface (Figure 6) and up through the troposphere. However, there is a lag between the warming of the tropical Pacific and its effect on global temperatures. The lag is longer in the troposphere than it is at the surface. Global surface temperatures might have been slightly elevated by the near-El Niño conditions that prevailed in late 2014. However, the full effect on global temperature of the strong 2015 El Niño is likely to continue after El Niño peaks.

Figure 7 shows a schematic of typical precipitation anomaly patterns that are favoured during El Niño. Figure 3 shows observed precipitation anomalies for 2015. Rainfall deficits consistent with El Niño were observed from Central America to northern Brazil, in southern parts of Africa, South-East Asia, large areas of Oceania and eastern Australia. Monsoon rains in India were also below average. Areas of above-average precipitation included southern Brazil and northern Argentina, and southern areas of the United States.

Moreover, El Niño affects the formation and development of tropical cyclones. It suppresses the formation of hurricanes in the North Atlantic and promotes the formation of hurricanes and typhoons in the Eastern North Pacific. That is consistent with observations from 2015 (see page 19).

CRYOSPHERE

In the northern hemisphere, the seasonal cycle of Arctic sea-ice extent usually peaks in March and reaches its minimum in September. Ever since consistent satellite records began in the late 1970s, there has been a general decline in sea-ice extent throughout the seasonal cycle. In 2015, the daily maximum extent, which occurred on 25 February, was the lowest on record, at 14.54 million km^2. That is 1.10 million km^2 below the 1981–2010 average and 0.13 million km^2 below the previous record set in 2011. The minimum sea-ice extent was recorded on 11 September. It measured 4.41 million km^2. That was the fourth-lowest minimum extent in the satellite record (Figure 8). On 30 December, unusually warm air moved northward into the polar region. Consequently, an above-freezing temperature of +0.7 °C was, albeit briefly,

ALASKA, UNITED STATES
Walruses haul out on land as a result of sea-ice decline.

NOAA

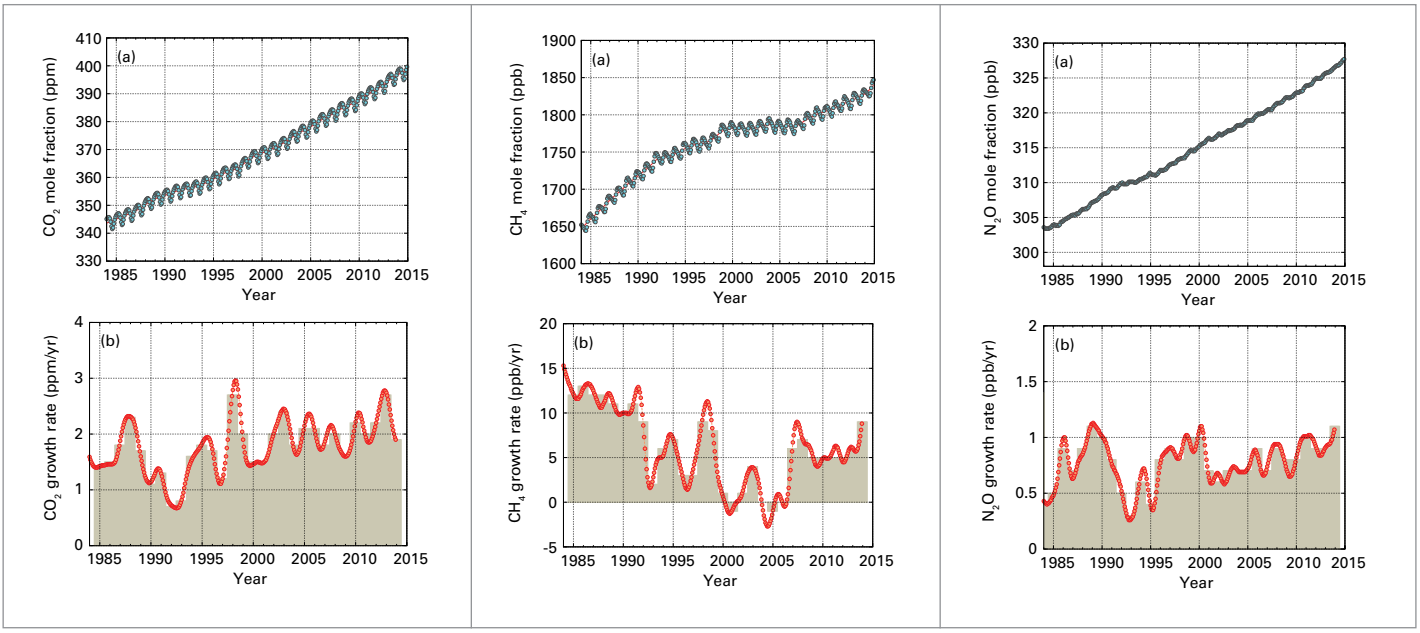

Figure 9. Globally-averaged mole fractions (a measure of concentration) of CO_2 in parts per million (left), CH_4 in parts per billion (middle) and N_2O in parts per billion (right); the period 1984–2014 is shown on the top row with growth rates on the bottom row; annually averaged growth rates shown as columns in the bottom row of plots

recorded on that day by a weather buoy near the North Pole.

In the southern hemisphere, the seasonal cycle of Antarctic sea-ice extent typically peaks around September or October and reaches a minimum in February or March. In 2015, a daily maximum extent of 18.83 million km^2 was recorded on 6 October. That is the sixteenth-highest maximum extent in the satellite record and 1.33 million km^2 below the 2014 record maximum. The minimum extent, recorded on 20 February, was 3.58 million km^2. That is the fourth-highest summer minimum extent on record and 0.17 million km^2 below the 2008 record. Compared with the long-term trend, there is considerable variability in the year-to-year Antarctic sea-ice minimum extent. In the past five years, both the second-highest (2013) and the third-lowest (2011) monthly extent have been recorded. Daily Antarctic sea-ice extent was at or near record levels early in the year. But in August, the extent moved close to the long-term average. There is low confidence in the scientific understanding of the observed long-term increase in Antarctic sea-ice extent since 1979.

In Greenland, the total extent of the summer melt area in 2015 was the eleventh-largest on record (since 1978) and about 85 000 km^2 above the 1981–2010 average. This is above the long–term average, but not unusual in the context of the past decade. The total extent of the highest summer melt on record (2012) was over 300 000 km^2 above the 1981–2010 average. At the Greenland summit station, run by the Danish Meteorological Institute, winter, spring and summer temperatures were below average. On 28 August, a new record low temperature of –39.6 °C was recorded for that month. On 24 October, the lowest recorded temperature of –55.2 °C equalled the current record low, which was reported on 31 October 2007.

GREENHOUSE GASES

The latest analysis of greenhouse gas observations from the WMO Global Atmosphere Watch programme shows that globally averaged mole fractions of carbon dioxide (CO_2), methane (CH_4) and nitrous oxide (N_2O) reached new highs in 2014 (Figure 9 – the latest information is from 2014 as there is a one-year lag in comprehensive reporting). In 2014, the globally averaged CO_2 mole fraction reached 397.7 ± 0.1 ppm.[2] That is 143% of the pre-industrial level. The annual increase from 2013 to 2014 was 1.9 ppm. That is close to the average annual increase for the last 10 years and higher than the average growth rate for the 1990s (about 1.5 ppm/year).

[2] ppm: parts per million; ppb: parts per billion

Preliminary NOAA data for 2015 indicate that the CO_2 increase of 3.01 ppm/year was a record. The increase in atmospheric CO_2 from 2003 to 2013 corresponds to about 45% of the CO_2 emitted by human activity with the remainder removed by the oceans and the terrestrial biosphere.

Atmospheric CH_4 reached a new high of 1833 ± 1 ppb in 2014. That is 254% of the pre-industrial level and is due to increased anthropogenic emissions. The average global N_2O mole fraction in 2014 reached 327.1 ± 0.1 ppb. That is 1.1 ppb above 2013 and 121% of the pre-industrial level (270 ppb). The annual increase from 2013 to 2014 was greater than the mean growth rate over the past 10 years (0.87 ppb/year).

The NOAA Annual Greenhouse Gas Index shows that, from 1990 to 2014, radiative forcing by long-lived greenhouse gases increased by 36%, with CO_2 accounting for about 80% of that increase. The increase in total radiative forcing by all long-lived greenhouse gases since pre-industrial times reached +2.94 W/m². The total radiative forcing by all long-lived greenhouse gases corresponds to a CO_2-equivalent mole fraction of 481 ppm.

REGIONAL EXTREMES

There were numerous extreme events recorded worldwide, with damages and casualties reported in several cases (Figure 11). This section summarizes high-impact weather and climate events which were recorded in the regions during the year.

REUTERS / Hani Amara

TRIPOLI, LIBYA
Heavy rains caused the closure of several main streets in the capital.

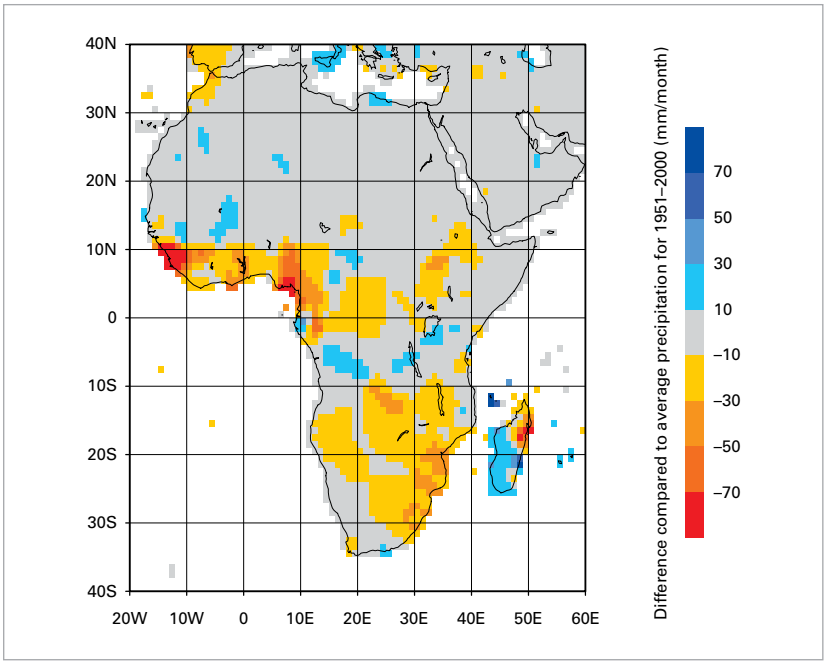

AFRICA

During the spring of 2015 in South Africa, record high temperatures were exceeded on a regular basis. On 27 October, a temperature of 48.4 °C was recorded at Vredendal: that was the highest temperature on record for South Africa. The heatwave continued in early November. All-time high temperatures of 40.3 °C at Pretoria and 36.5 °C at Johannesburg were recorded.

High temperatures also affected many places in northern Africa. In Morocco, new temperature records for the month of May were set at some stations, and extreme heat in July led to a nearly 50% reduction in citrus fruit production. In Egypt, maximum temperatures in July reached 47.6 °C at Luxor. In West Africa, May was unusually warm in Burkina Faso and Niger, being 3 °C above average in places.

In February, heavy rain affected North Africa. At Alhoceima in Morocco, the normal monthly rainfall is 36 mm. In February, 206 mm of rain was recorded, of which 88 mm fell in 24 hours on 18 February. Heavy rain also affected the western coastal region of Libya in September. Flash floods occurred at Sorman when more than 90 mm of rain fell in 24 hours: the monthly average is 8 mm. From September to the end of the year, severe drought conditions affected Morocco.

Figure 10. Annual precipitation anomalies (difference from 1951–2000 average) in mm/month for Africa in 2015
(Source: Global Precipitation Climatology Centre, Germany)

Figure 11. Climate extremes in 2015

(Source: Map and information provided by the National Climatic Data Center, NOAA, United States, http://www.ncdc.noaa.gov/sotc)

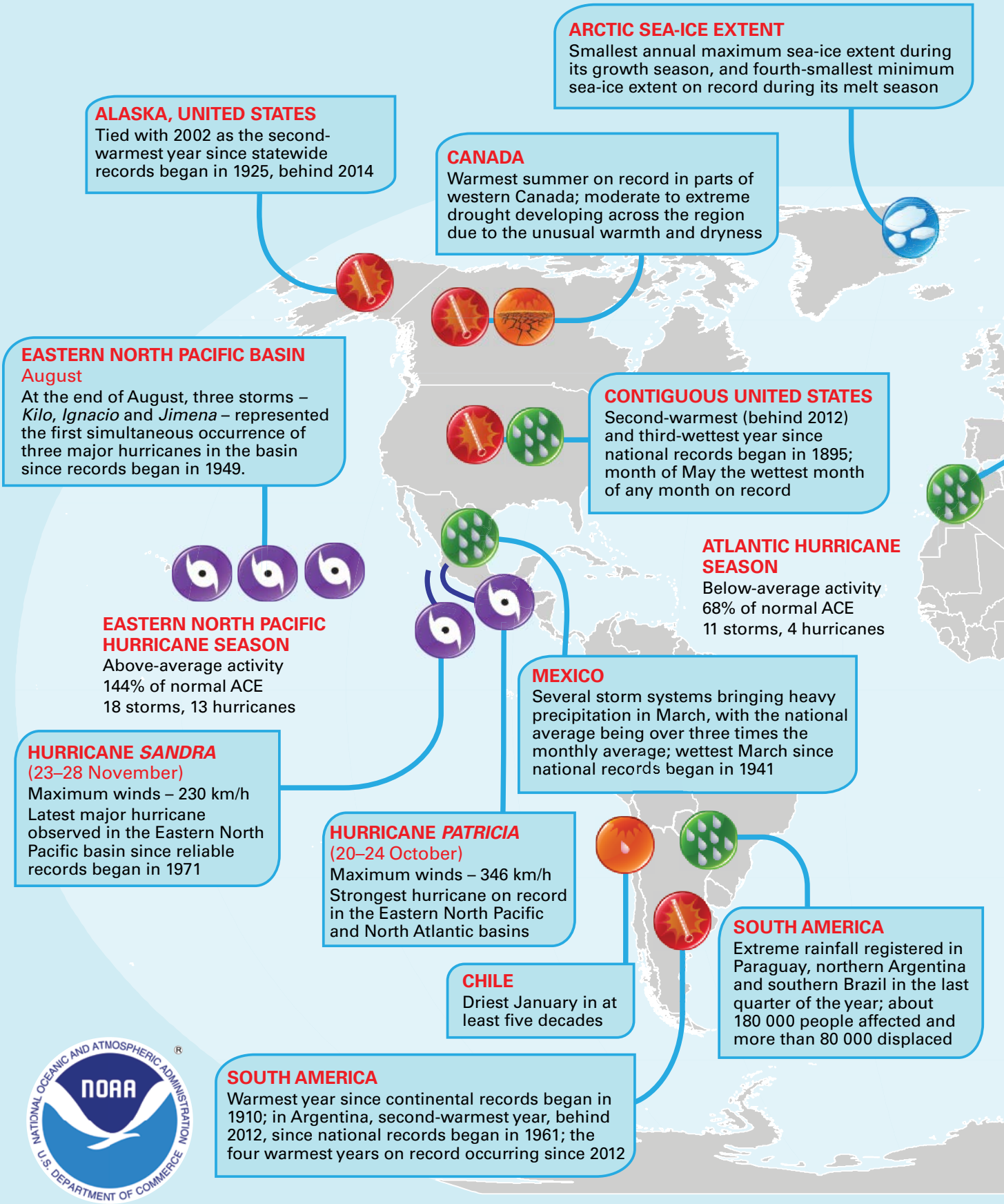

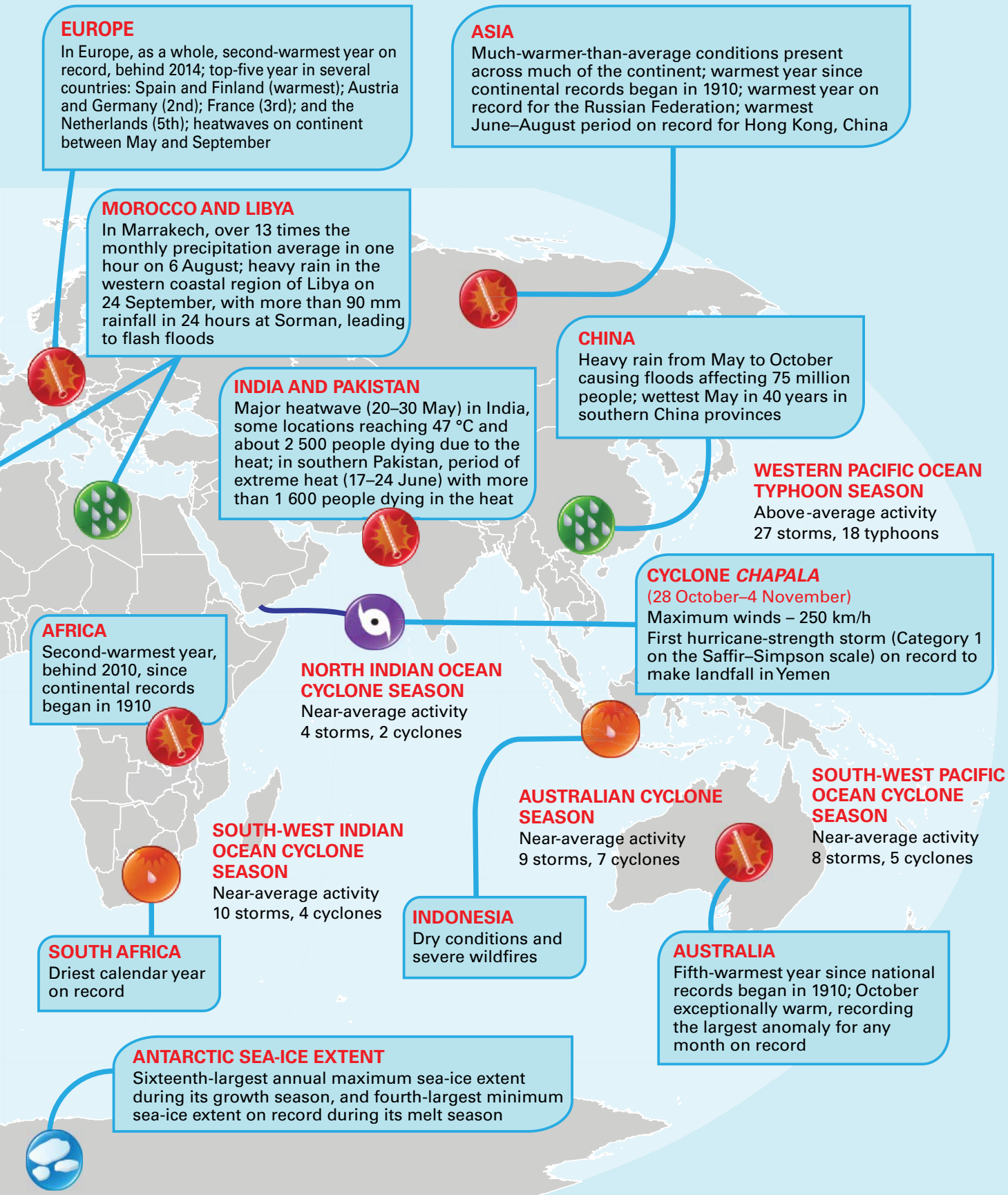
EUROPE
In Europe, as a whole, second-warmest year on record, behind 2014; top-five year in several countries: Spain and Finland (warmest); Austria and Germany (2nd); France (3rd); and the Netherlands (5th); heatwaves on continent between May and September
ASIA
Much-warmer-than-average conditions present across much of the continent; warmest year since continental records began in 1910; warmest year on record for the Russian Federation; warmest June–August period on record for Hong Kong, China
MOROCCO AND LIBYA
In Marrakech, over 13 times the monthly precipitation average in one hour on 6 August; heavy rain in the western coastal region of Libya on 24 September, with more than 90 mm rainfall in 24 hours at Sorman, leading to flash floods
CHINA
Heavy rain from May to October causing floods affecting 75 million people; wettest May in 40 years in southern China provinces
INDIA AND PAKISTAN
Major heatwave (20–30 May) in India, some locations reaching 47 °C and about 2 500 people dying due to the heat; in southern Pakistan, period of extreme heat (17–24 June) with more than 1 600 people dying in the heat
WESTERN PACIFIC OCEAN TYPHOON SEASON
Above-average activity
27 storms, 18 typhoons
CYCLONE CHAPALA
(28 October–4 November)
Maximum winds – 250 km/h
First hurricane-strength storm (Category 1 on the Saffir–Simpson scale) on record to make landfall in Yemen
AFRICA
Second-warmest year, behind 2010, since continental records began in 1910
NORTH INDIAN OCEAN CYCLONE SEASON
Near-average activity
4 storms, 2 cyclones
AUSTRALIAN CYCLONE SEASON
Near-average activity
9 storms, 7 cyclones
SOUTH-WEST PACIFIC OCEAN CYCLONE SEASON
Near-average activity
8 storms, 5 cyclones
SOUTH-WEST INDIAN OCEAN CYCLONE SEASON
Near-average activity
10 storms, 4 cyclones
INDONESIA
Dry conditions and severe wildfires
SOUTH AFRICA
Driest calendar year on record
AUSTRALIA
Fifth-warmest year since national records began in 1910; October exceptionally warm, recording the largest anomaly for any month on record
ANTARCTIC SEA-ICE EXTENT
Sixteenth-largest annual maximum sea-ice extent during its growth season, and fourth-largest minimum sea-ice extent on record during its melt season

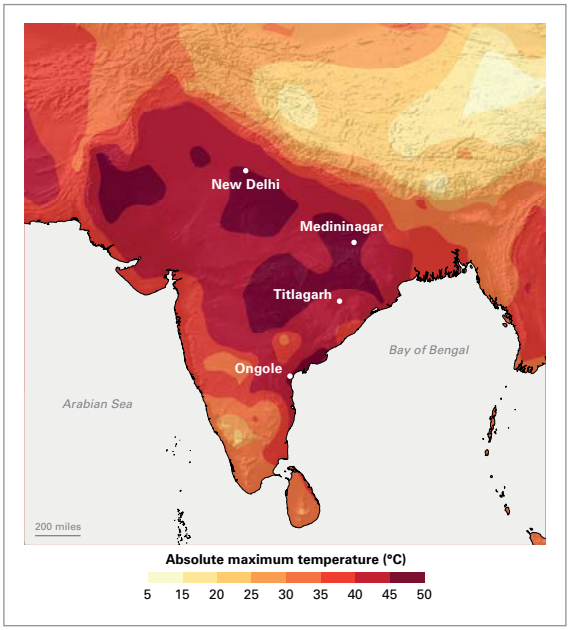

Figure 12. Maximum temperatures during the period 24–30 May 2015 *(Source: NOAA, United States, Climate.gov based on interpolated weather station data provided by the India Meteorological Department)*

The West African monsoon brought significant flooding. Heavy rain led to flooding in July and August, affecting about 21 000 people in Burkina Faso. In Niger, despite total rainfall for the year that was close to the long-term mean, heavy rain (more than 100 mm in 24 hours) was recorded at a number of locations and led to floods that killed 25 people. Heavy rains and floods also affected Gambia and Mali (Figure 10).

Further south, in the United Republic of Tanzania, heavy rain and floods affected the country in March, May and November. Several extreme rainfall events, with record-breaking daily totals, were associated with the deaths of more than 50 people. In the South-West Indian Ocean, Mauritius had its wettest June since 1976. Total rainfall for the month was 180% of the long-term average. Heavy rain in January also led to flooding in Malawi, Mozambique and Zimbabwe.

In South Africa, the season from July 2014 to June 2015 was, on average, the driest since 1991/1992 and the third-driest since 1932/1933. By the end of the summer, the prolonged drought conditions had severely affected the maize, sugar cane and sorghum harvests. As a whole, 2015 was the driest calendar year on record.

ASIA

Major heatwaves affected the Indian subcontinent in 2015. In May, some stations in Odisha, Telangana and coastal Andhra Pradesh reported temperatures of about 47 °C between 23 and 26 May (Figure 12). About 2 500 people died due to the heat, with over 2 000 deaths in the south Indian states of Telangana and Andhra Pradesh alone. A period of extreme temperatures also affected southern Pakistan from 17 to 24 June, where temperatures exceeded 40 °C. More than 1 400 people died in the heat of Karachi and about 200 people in other parts of Sindh province. Extreme heat is common in the pre-monsoon season on the Indian subcontinent. But in 2015, the heat extended over a larger area than normal. It incorporated regions such as Andhra Pradesh in eastern India and coastal Pakistan, and was accompanied by very high humidity in places.

KARACHI, PAKISTAN

People cool off from the heat with water from a leaking pipeline.

REUTERS / Akhtar Soomro

On 31 July, Bandar Mahshahr, a coastal city in the Islamic Republic of Iran, recorded a temperature of 46 °C combined with a dewpoint temperature of 32 °C. High temperature combined with high humidity is exceptional. The Hong Kong Observatory reported its warmest summer since records began in 1884. On 8 August, the temperature at the Observatory reached 36.3 °C, beating the previous record of 36.1 °C set in 1990.

A mixture of dry conditions and heavy rainfall episodes affected the Indian subcontinent in 2015. For India, the total rainfall recorded during the Indian summer monsoon between June and September was 86% of its long-term average. India also experienced below-average rainfall in 2014, the fourth time that two consecutive

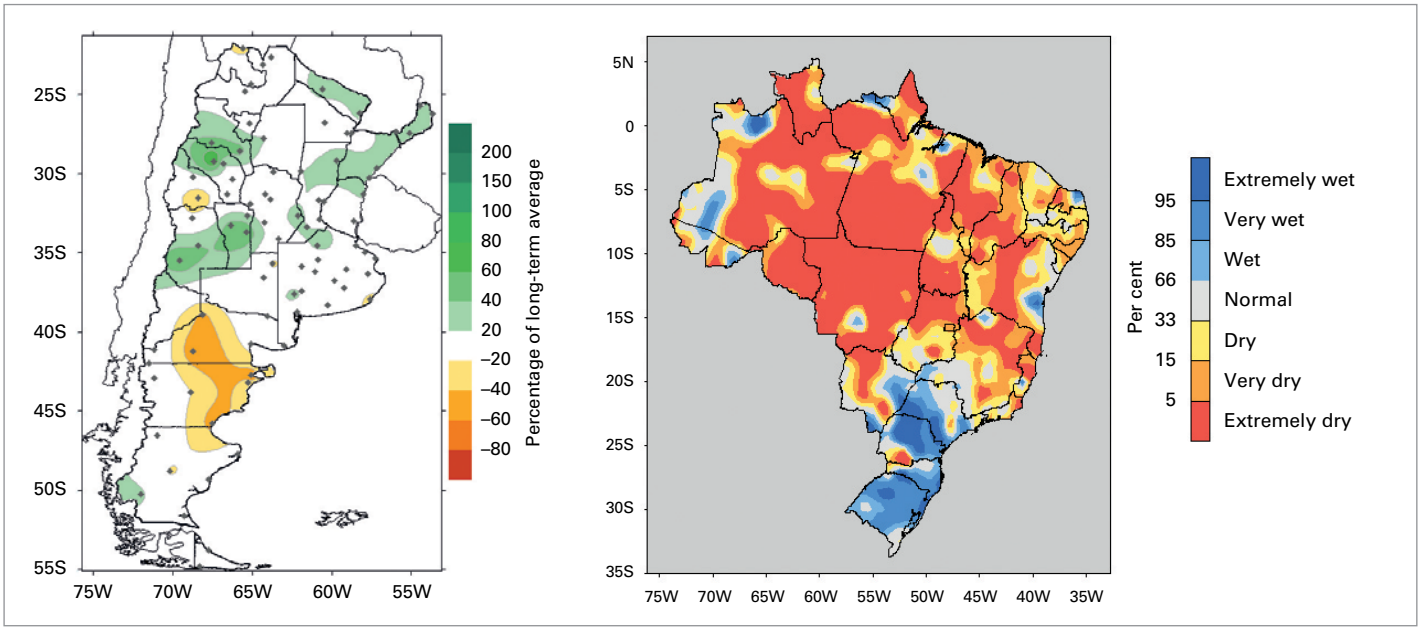

Figure 13. Annual precipitation anomalies for Argentina (left) expressed as a percentage of the long-term average and standardized precipitation anomalies for Brazil (right) for 2015 *(Sources: Servicio Meteorológico Nacional, Argentina and Instituto Nacional de Meteorologia, Brazil)*

below-average rainfall years occurred since records began 115 years ago. At the other extreme, heavy monsoon rains during 2015 led to flooding which killed over 200 people, mainly in West Bengal and Assam. Exceptionally heavy rain over Tamil Nadu and coastal Andhra Pradesh in November and early December led to flooding which killed more than 100 people.

In Pakistan, the summer monsoon was erratic. Ninety per cent of the seasonal total was concentrated over the first half of the season in areas which the rain seldom reaches. The station at Mianwali recorded 340 mm of rain in 36 hours on 2 and 3 August; the monthly average is 115.9 mm. Pakistan also saw unseasonal weather during March and April, with heavy rain and late frost damaging crops. A rare tornado hit the Peshawar valley on 27 April and killed 45 people.

Compared to the past 15 years, China underwent lower levels of weather-related mortality and fewer areas were affected by extreme weather. Between May and September, China experienced 35 heavy rain events. Subsequent flooding affected 75 million people with estimated economic losses of US$ 25 billion. Between 5 and 31 May, over 150% of the long-term average rainfall fell in Huanan County. That was slightly more than 2014 and the most rain recorded in nearly 40 years. However, North China, the east part of North-West China and Liaoning Province were dominated by serious and successive droughts during the summer and autumn. Maize and potato crops were seriously affected.

Drought over the European part of the Russian Federation during the late spring and summer led to crop failures over more than 1.5 million hectares, with associated economic losses of about 9 billion roubles. Particularly affected were: the Volgograd and Saratov regions along the Volga river, the Orenburg region to the east and the Republic of Kalmykia in the southern area of the European part of the Russian Federation. In the Asian part of the Russian Federation, drought was recorded in Buryatia during the late spring and summer, while both Buryatia and Transbaikalia experienced forest fires that burned about 460 000 and 880 000 hectares respectively.

SOUTH AMERICA

Temperatures in 2015 were above normal for most of the continent, with anomalies of up to 2 °C. The highest temperatures were recorded in the Bolivarian Republic of Venezuela and Colombia on the Caribbean coast, northern Chile and south-eastern Brazil. After a remarkably warm austral autumn and winter, during which several records were set, Argentina experienced

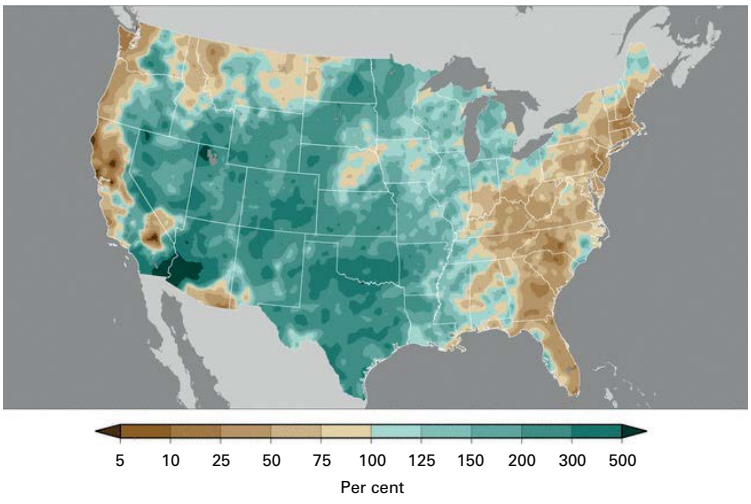

Figure 14.
Precipitation anomalies in the United States for May 2015 expressed as a percentage of the twentieth century average
(Source: National Centers for Environmental Information, NOAA, United States)

a colder-than-normal spring and its coldest October on record. However, for the country as a whole, 2015 was the second-warmest year on record.

Reduced rainfall over Brazil and northern areas of South America is common during an El Niño. Brazil started the year with a drought in its southern and eastern areas. The drought shifted north, with scant rainfall during the dry season over the Amazon (Figure 13). The persistently dry conditions in Colombia and the Bolivarian Republic of Venezuela had a severe impact on agriculture, raising cattle and hydropower generation during the last quarter of the year.

In January, Chile was drier than average throughout the country, with the south of the country seeing the most extreme deficits. In some places, it was the driest January in at least 50 years. The stations at Temuco and Valdivia, situated halfway down the country, recorded no rainfall for the whole month. In the Patagonia region of southern Argentina, the above-normal temperatures and below-normal rainfall at the beginning of 2015 provided the ideal conditions for one of the largest wildfires in the history of Argentina. The fire lasted nearly two months and affected 41 000 hectares of native forests.

In February and March, heavy rain affected a number of places in South America, including through flooding. A number of long-running weather stations in Argentina broke their February precipitation records. The Córdoba Observatory recorded 385 mm of rain for the month, beating a long-standing record of 266 mm set in 1889. In March, there were unusually heavy rains in the northern part of Chile in the Atacama Region, which caused flooding and mudslides in cities such as Copiapó and Chañaral. By contrast, dry conditions prevailed further south.

In the last quarter of 2015, extreme rainfall was recorded in several parts of South America, particularly in Paraguay, northern Argentina and southern Brazil. About 180 000 people were affected by flooding and more than 80 000 people were displaced.

NORTH AMERICA, CENTRAL AMERICA AND THE CARIBBEAN

Western Canada and the United States were unusually warm. It was the second-warmest year on record for the contiguous United States, and four states had their warmest year on record. Record high winter average temperatures were also reported along the Pacific coast of Canada. And although February was the second-coldest on record for some states of the United States, December saw record high temperatures in 29 states.

Low annual rainfall, associated with the influence of El Niño, were widespread throughout Central America and the Caribbean. Rainfall totals for Puerto Rico were below the long-term average and led to drought and water rationing in some areas.

The dry and warm conditions that prevailed across much of the western United States during the year provided ideal conditions for wildfires. In Alaska, over 400 fires burned 728 000 hectares of land in May, breaking the previous record of 216 fires and 445 000 hectares. Over 700 wildfires were reported in Alaska during July, and nearly 2 million hectares were burned during the summer. Large fires burned throughout the North-West in August. The Okanogan Complex fire was Washington's largest on record and spread over more than 121 000 hectares.

It was the wettest May on record for the contiguous United States and the wettest month overall in 121 years of record keeping (Figure 14).

Colorado, Oklahoma and Texas each had record precipitation during the month. The May rains effectively ended the drought that had affected the southern plains since 2011. Further west, however, long-term drought conditions continued. Basins across the West depend on snowpack as a water resource. On 1 April, the snow water equivalent was 5% of normal levels in the West – the lowest since measurements began in 1950. The previous lowest snow water equivalent was 25% of normal levels, recorded in 1977 and 2014.

In early October, as Hurricane *Joaquin* moved off the east coast, it interacted with a low pressure system and pulled tropical air into the Carolinas. Record five-day rainfall totals of 380–630 mm were widespread. There was significant flooding across the region, which killed 16 people. Extreme rainfall and flash flooding, some of it associated with the remnants of Hurricane *Patricia*, also affected parts of Texas. It was both the wettest and the warmest December on record for the contiguous United States.

Mexico had its wettest March since records began in 1941. Rainfall across the country was 69.6 mm, well above the long-term average of 14.7 mm. Baja California and Baja California Sur had their wettest June on record and Sonora had its second-wettest. In the centre and the north of the country, Aguascalientes and Zacatecas had their third-wettest June.

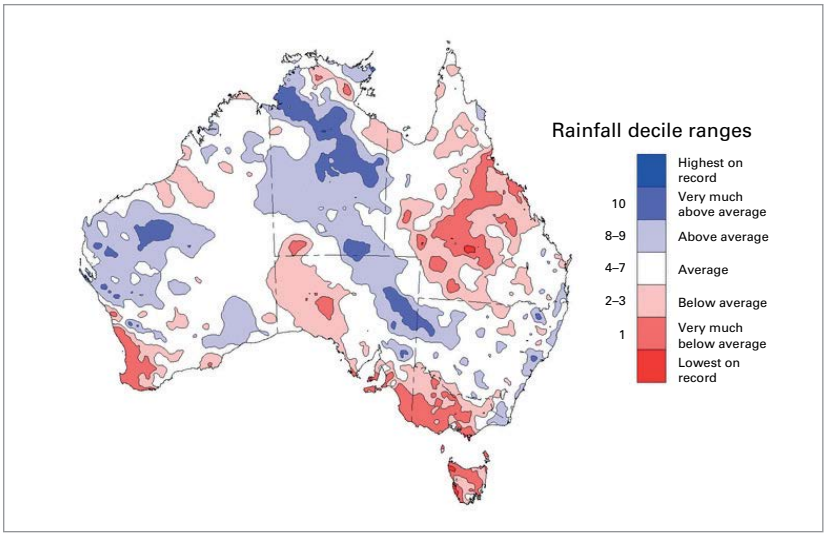

Figure 15. Australian annual total precipitation for 2015 expressed as deciles of the observed distributions *(Source: Bureau of Meteorology, Australia)*

SOUTH-WEST PACIFIC

In Indonesia, the low rainfall associated with El Niño increased the risk and incidence of wildfires, which in turn led to poor air quality. In the first half of the year, 40 provinces in upper Thailand experienced their second-lowest total rainfall in 64 years.

Australia had its warmest October on record. The anomaly for October was also the highest anomaly for any month since records began. A heatwave early in the month set new records for early-season warmth in southern Australia. It was the fifth-warmest year on record as a whole.

Overall, Australia was about 4% drier than average in 2015. But that encompassed both areas with much higher-than-average rainfall and areas which were much drier than average (Figure 15). The El Niño in 2015 likely contributed to below-average rainfall over eastern Australia (Figure 7), moderated by changes of sea-surface temperature in the Indian Ocean (the Indian Ocean Dipole was positive between August and November). Since the end of the most recent La Niña in early 2012, a series of dry years has seen long-term drought re-emerge in western Victoria, South Australia and south-west Western Australia.

ALASKA, UNITED STATES

Over 700 wildfires were reported in Alaska during July, and nearly 2 million hectares were destroyed during the summer.

Sherman Hogue / Fort Wainwright PAO

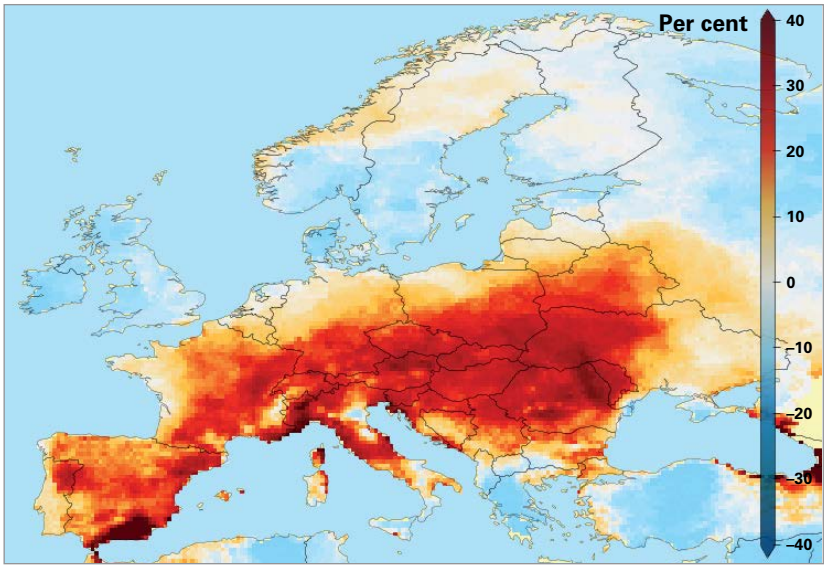

Figure 16. Percentage of warm days (exceeding the 90th percentile of the reference period, 1981–2010) relative to average during European summer 2015 *(Source: Royal Netherlands Meteorological Institute)*

In New Zealand, annual rainfall totals were below normal in some areas, such as Kaitaia and Kerikeri, both of which had their driest year on record. But rainfall was near normal for the rest of the country.

EUROPE AND THE MIDDLE EAST

Heatwaves affected Europe from May through September (Figure 16). Monthly average records were set in July for Austria and Spain. The heat was often intense. Kitzingen in Germany set a new record for the country of 40.3 °C on 5 July. In May, 42.6 °C was recorded at Lanzarote airport and Valencia airport in Spain: that exceeded both their previous highest May temperatures by 6 °C. In France, Spain and Poland, a number of stations broke records for their highest temperatures. The United Kingdom set a new July temperature record of 36.7 °C on 1 July. From 1 to 4 August, Jordan saw temperatures of nearly 8 °C above normal, reaching 47 °C at Wadi Elrayyan. Seven stations in Bosnia and Herzegovina reported new September temperature records in the six days from 15 September. The Republic of Moldova and Serbia both saw record daily temperatures for September. In Israel, the minimum temperature at Sedom on 9 September was 36.5 °C. That is the highest daily minimum temperature ever recorded in Israel and breaks a record set in Tiberias in 1936 of 36 °C. As far east as Azerbaijan, temperature records were set at certain stations between June and September.

In some cases, the heatwaves were unusual in their duration. In May, the maximum temperature at Beja in Portugal was above 30 °C for 19 days; on average, temperatures exceed that level in Beja for 5 days. At Slap in the Vipava valley in Slovenia, temperatures in excess of 30 °C were recorded on 54 days between June and August. In Spain, a heatwave from 27 June to 22 July was by far the longest on record. Between June and August, Slovenia experienced 5 heatwaves. Ljubljana reported a record run of 21 days with temperatures of above 30 °C. Hungary had 41 days above 30 °C during the summer, 22 days more than its average.

November and December were unusually warm over Europe. December was the warmest on record for a number of countries including the United Kingdom, France, Germany and the Netherlands. In the Central England Temperature series it was the warmest December since at least 1659. Both Finland and the United Kingdom had their warmest recorded November days, while Estonia, Finland and the Republic of Moldova had their warmest recorded December days.

January was wet throughout large parts of Northern Europe and Scandinavia. In western parts of Finland, many weather stations reported record high precipitation totals for the month. In Sweden, 134.6 mm of rain fell in Piteå in January, making it the wettest January since at least 1860. Widespread heavy rain on Cyprus caused flooding and landslides. In February, heavy rain affected countries in southern Europe with flooding in parts of Albania, the former Yugoslav Republic of Macedonia, Greece and Bulgaria.

In Spain, 300 mm of rain fell in some areas of Castellón Province between 20 and 24 March. In May, Sweden was very wet across almost the entire country. Several stations with rainfall records going back more than 100 years hit their monthly records. In Stockholm, it was the wettest May in 200 years. Finland, Norway and Denmark had their second-wettest May on record.

France saw three periods marked by particularly heavy rainfall. The first was 23–24 August, when 108.1 mm of rain fell in one hour in Montpellier, Languedoc region. That is the

PORT VILA, VANUATU
A boy runs past books laid to dry in the sun after the roof of the Central School library was blown away by Cyclone *Pam*.

REUTERS / Edgar Su

highest one-hour total recorded at the site. From 12 to 13 September, a number of stations recorded rainfall totals in excess of 200 mm. On 3 October, close to 200 mm of rain fell in two hours in parts of the Alpes-Maritimes region and 20 people were killed.

In September, Irish stations in Galway and Mayo saw record daily rainfall levels of over 100 mm on 11 and 13 September, which led to flooding. In mid-October, heavy rain in Bosnia and Herzegovina led to flooding in Mostar and Stolac City. In December, the United Kingdom had its highest ever 24-hour rainfall total (341.4 mm at Honister Pass in Cumbria in the 24 hours to 1800 GMT on 5 December 2015) and its wettest December on record.

Some areas were particularly dry. In April, there were very dry conditions in Austria: Klagenfurt experienced its second-driest April since 1813, which led to forest fires. Between late May and mid-August, some western parts of Slovakia recorded their lowest rainfall totals since 1872. In July, parts of France experienced record low monthly precipitation. Large areas of Serbia experienced extreme drought in July. Estonia had its driest October since 1961. Austria had its second-driest December since 1858, and Hungary its third-driest since 1901.

TROPICAL CYCLONES

Globally, a total of 91 tropical storms formed during 2015. A named storm is defined as a tropical storm where the wind speed equals or exceeds 63 km/h. The figure of 91 storms is above the 1981–2010 annual average of about 85 storms, and slightly above the seventy-fifth percentile of 90 storms. The lowest number of storms in a year in the modern satellite era was 67 in 2010.

In the **North Atlantic** basin, there were 11 named storms, of which 4 became hurricanes; 2 of these (*Danny* and *Joaquin*) were classified as major hurricanes. This is slightly below the long-term average of 12 storms, 6 hurricanes and 3 major hurricanes. Hurricane activity in the North Atlantic is typically suppressed during an El Niño. Accumulated Cyclone Energy (ACE) is a measure of the combined strength and duration of tropical storms. In 2015, the ACE for the Atlantic basin was about 68% of the long-term average.

In the **Eastern North Pacific** basin, 18 named storms formed; 13 of these storms became hurricanes and 9 became major hurricanes. The 1981–2010 averages for a year are 15 storms, 8 hurricanes and 4 major hurricanes. Hurricane

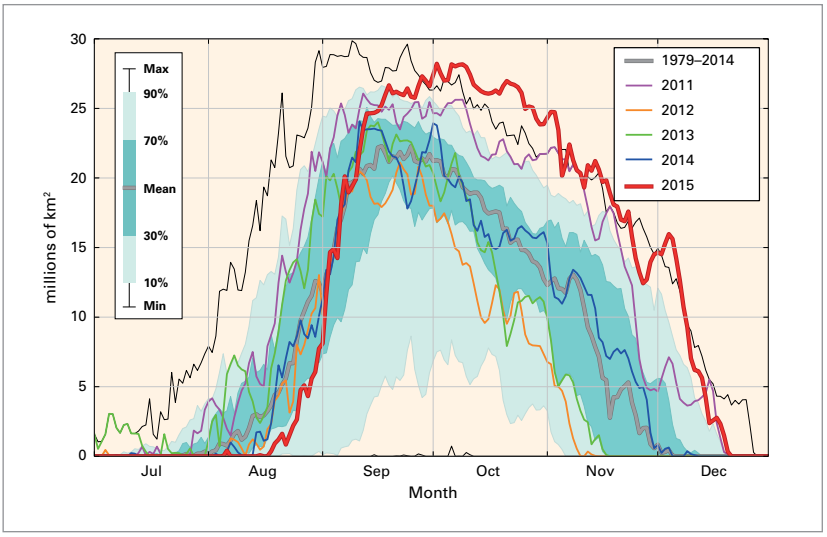

Figure 17. Area (millions of km²) where the total ozone column is less than 220 Dobson units, with 2015 shown in red and other years characterized by large ozone holes shown for comparison. The thick grey line is the 1979–2014 average, with the dark and light green-blue shaded areas representing the 30th to 70th percentiles and 10th and 90th percentiles, respectively, and the thin black lines showing the maximum and minimum values for each day during the 1979–2014 time period. The plot is produced at WMO based on data from the National Aeronautics and Space Administration Ozonewatch website (http://ozonewatch.gsfc.nasa.gov), which are based on satellite observations from the OMI and TOMS instruments.

Patricia (20–24 October) was the strongest hurricane on record in either the Atlantic or eastern North Pacific basins, with maximum sustained wind speeds of 346 km/h. It made landfall on the Mexican coast on 24 October with 241 km/h winds in a sparsely populated area. The remnants of *Patricia* contributed to heavy rainfall and flooding in the southern plains of the United States and the lower Mississippi river valley. The ACE for the Eastern North Pacific was about 44% higher than the long-term average and was the highest in the basin since 1993. The Central Pacific region experienced 7 named storms in total, 3 of which reached hurricane strength.

In the **Western North Pacific** basin, 27 named storms were recorded. Of these, 18 reached typhoon strength. The estimated averages for the whole year are 26 storms and 17 typhoons. Typhoon *Koppu*, known locally as *Lando*, made landfall in the Philippines in October, affecting many people and causing widespread damage. Because of the tracks taken by the storms, no storm warnings were issued in Hong Kong, China in August and September for the first time since 1946. Six typhoons made landfall over China. Typhoons *Chan-hom*, *Soudelor* and *Mujigae* led to combined estimated economic losses of US$ 8 billion.

In the **North Indian Ocean,** 4 named storms formed, compared with an annual average of 5. *Komen* developed as a tropical depression over the north-eastern part of the Bay of Bengal near the coast of Bangladesh. It strengthened at sea before making landfall as a tropical storm. Rainfall associated with the storm and monsoon rains led to severe flooding and landslides in Myanmar. Bangladesh also suffered from flash floods and landslides. The storm came after an earlier period of heavy rains from 24 June. Tropical cyclone *Chapala* made landfall in Yemen and led to substantial flooding. This was the first tropical cyclone to make landfall in Yemen at hurricane strength during the satellite era. Socotra Island was affected by both cyclones *Megh* and *Chapala*. *Megh* developed shortly after *Chapala* made landfall. *Chapala* was a Category 3 storm when it passed to the north of Socotra Island, while *Megh* was Category 2.

In the **South-West Indian Ocean**, 10 named storms developed during the 2014/2015 season, slightly above the long-term average of 9. Of these, 4 reached tropical cyclone strength and 2 became intense tropical cyclones. In the calendar year 2015, which contains the end of one season and the start of another, 11 named storms formed.

In the **Australian** basin, the 2014/2015 season saw 9 named storms develop. There were 7 named storms during 2015, comprising the end of one season and the start of another. That was slightly below the long-term average of 10. Cyclone *Marcia* was the most intense cyclone to make landfall that has been observed so far south on the east coast, at least in the modern satellite era. It was unusual that *Raquel* occurred at the end of June. Such a late storm in the eastern Australian region has not previously been recorded in the satellite era. The only previously recorded winter cyclone was in early June 1972.

There were 11 named storms in the **South-West Pacific**. The annual average is 6. Tropical cyclone *Pam* made landfall over Vanuatu as a Category 5 cyclone on 13 March and destroyed many homes. The Government of Tuvalu declared a state of emergency on 13 March after severe inundations from the storm surge and sea swell. Kiribati reported severe damage on its three southern islands. The Solomon Islands were also affected. There were 8 named storms during the 2014/2015 season.

OZONE-DEPLETING SUBSTANCES

Due to the success of the Montreal Protocol on Substances that Deplete the Ozone Layer, the use of halons and chlorofluorocarbons has been discontinued. However, these compounds will remain in the atmosphere for many decades because of their long lifetime. There is still more than enough chlorine and bromine in the atmosphere to cause the complete destruction of ozone at certain altitudes in Antarctica from August to December. As a result, the size of the ozone hole from one year to the next is mostly governed by meteorological conditions.

During the austral winter and spring of 2015, temperatures in the stratosphere were colder than the long-term average (1979–2014). The southern polar vortex was particularly stable and concentric around the South Pole. The area encircled by the vortex was larger than usual, and the average for October was the largest on record, according to ERA Interim data from the European Centre for Medium-Range Weather Forecasts. Consequently, the onset of ozone depletion was delayed.

However, once ozone depletion started in mid-August, it proceeded rapidly. The area of the ozone hole reached its seasonal maximum of 28.2 million km^2 on 2 October, according to analysis by NASA (Figure 17). An analysis carried out at the Royal Netherlands Meteorological Institute (KNMI) shows that the 2015 ozone hole area reached a maximum of 27.1 million km^2 on 9 October. Thus the ozone hole was either the fourth- or fifth-largest on record after 2000, 2003 and 2006 in both analyses, as well as 1998 in the KNMI analysis.

Data from NASA indicate that, for the 60 consecutive days in 2015 when the ozone hole was at its largest, the average area of the hole was 25.6 million km^2. By that measure, the 2015 ozone hole was the largest on record. In the KNMI analysis, the equivalent area was 24.2 million km^2. That makes the 2015 ozone hole the joint second largest, equal with 1998 and behind 2006.

Ocean heat content increase reveals unabated global warming

Matthew D. Palmer,[3] Susan Wijffels,[4] John A. Church[4]

In a stable climate, the amount of energy that the Earth system absorbs from the Sun is balanced by the amount of energy emitted back to space by the Earth as thermal infrared radiation. However, increases in greenhouse gas concentrations have created an imbalance by reducing the emitted radiation and causing energy to accumulate in the Earth system over time. The rate of energy increase in the climate system – Earth's energy imbalance – is the most fundamental metric that defines the rate of global climate change.

On timescales longer than about a year, the vast majority (more than 90%) of Earth's energy imbalance goes into heating the oceans. Thus tracking ocean temperatures and associated changes in ocean heat content (OHC) allow us to monitor variations in Earth's energy imbalance over time. Observations of OHC have been pivotal for the assessment of climate models and the detection and attribution of human climate change. They are also essential to "anchor" satellite-based estimates of changes in Earth's energy imbalance.

As the oceans warm, they expand, resulting in both global and regional sea-level rise. Increased OHC accounts for about 40% of the observed global sea-level increase over the past 60 years and is expected to make a similar contribution to future sea-level rise. The warming of ocean waters adjacent to the ice sheets can also affect the flow of ice into the ocean, which is another key component of sea-level rise. Therefore, monitoring global and regional OHC, along with tide gauges and satellite measurements of sea level and ocean mass, is essential for understanding historical and future sea-level change.

In the past, one of the challenges for estimating the rate of OHC change has been the historical sparseness of the ocean observing system. Ocean subsurface temperature measurements have mostly relied on ship-based instruments, which often sample only the upper few hundred metres. As a result, many historical estimates of global OHC change are limited to about the upper 700 m, with large uncertainties prior to the 1970s, when widespread ocean sampling became possible through more affordable observing technologies.

The early 2000s saw a revolution in our ability to monitor global OHC and freshwater content through the inception of the Argo array of autonomous profiling floats. This array reached maturity in 2006 with approximately 3 000 floats distributed around most of the globe; they measure temperature and salt content over the upper 2 km of the oceans every 10 days. The Argo observations usher in a new era of monitoring Earth's energy imbalance and the various factors that shape its evolution over time.

While ocean temperatures below 300 m (Figure 18 b, c and d) show a relatively steady increase over the period 2006–2015, ocean surface temperatures (Figure 18 a) show additional multi-year variability primarily due to variation in the tropical Indian Ocean and Pacific Ocean associated with the El Niño Southern Oscillation. Most of these near-surface oscillations are balanced by deeper, opposing changes between 100 m and 300 m, and the 0–2 000-metre OHC rises steadily across this period. Land-surface temperatures show more variability again, with particularly large variations from year to year. According to estimates shown in Figure 18 e, between 75% and 99% of the warming occurs in the southern hemisphere, predominantly between 30°S and 50°S.

The observed OHC increase implies that Earth's energy imbalance is nearly constant at 0.65–0.80 W/m^2, expressed as an average value over the surface area of the planet. About 75%–80% of this value comes from the upper 2 000 m, as illustrated in Figure 18, with the remaining 20%–25% coming from the deeper ocean. The observed energy imbalance inferred by OHC change is within the range of 0.6–1.0 W/m^2 projected for the 2006–2015 period using climate models.

---

[3] Met Office Hadley Centre, Exeter, United Kingdom

[4] CSIRO Marine and Atmospheric Research, Hobart, Australia

Monitoring OHC enables us to better track the underlying rate of climate change on decadal and shorter timescales and to better quantify the effect of other climatic factors on Earth's energy imbalance, such as changes in man-made and volcanic aerosols. While Argo observations are currently limited to the upper 2 000 m of ocean depths, the technology now exists to profile over nearly the full ocean depth (up to 6 km). These new observations will become essential for monitoring climate and sea-level change as the impact of Earth's energy imbalance becomes apparent at ever greater depth in the global oceans.

References:

Wijffels, S. et al., 2016: Ocean temperatures chronicle the ongoing warming of Earth. *Nature Climate Change*, 6:116–118, doi:10.1038/nclimate2924.

von Schuckmann, K. et al., 2016: An imperative to monitor Earth's energy imbalance. *Nature Climate Change*, 6:138–144, doi:10.1038/nclimate2876.

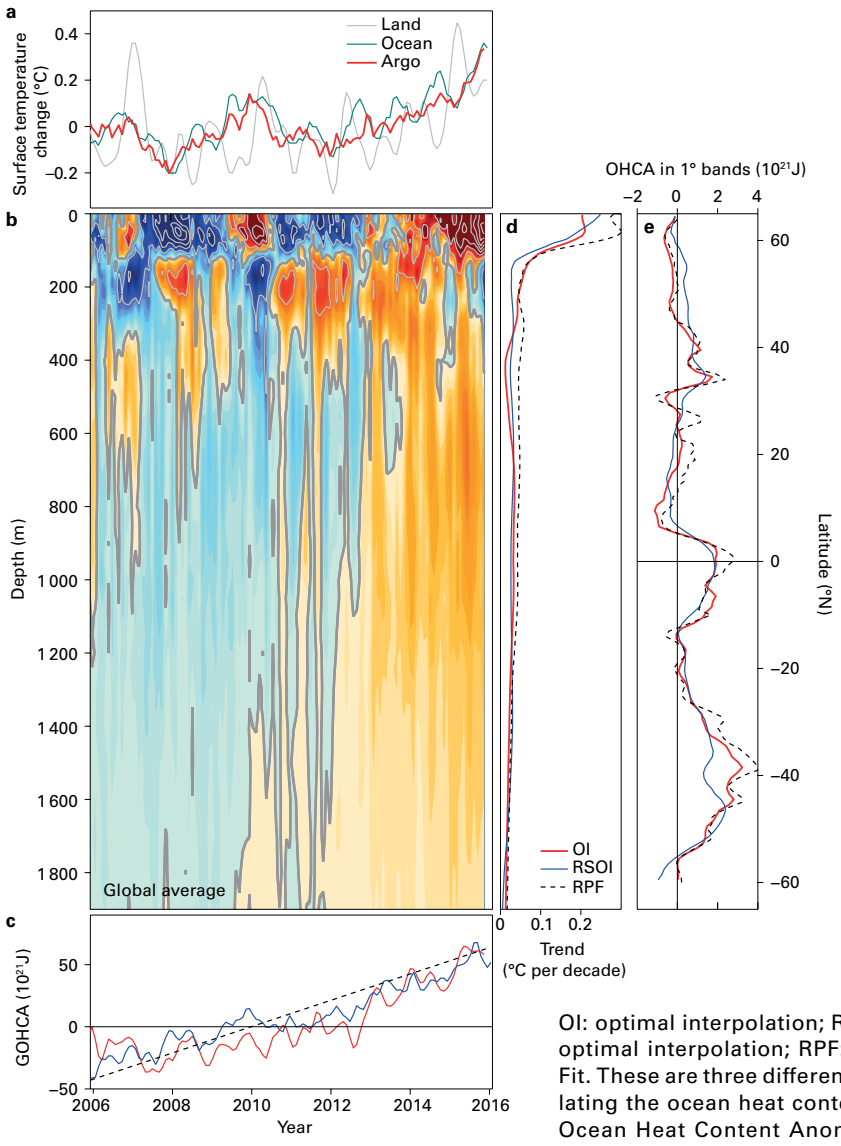

OI: optimal interpolation; RSOI: reduced space optimal interpolation; RPF: Robust Parametric Fit. These are three different methods for calculating the ocean heat content. GOHCA: Global Ocean Heat Content Anomaly; OHCA: Ocean Heat Content Anomaly.

Figure 18. (a) Globally averaged ocean surface temperature change (°C), from Argo (red), the National Oceanic and Atmospheric Administration (NOAA, turquoise) and a six-month running mean of NOAA globally averaged land temperature change (grey); (b) Global average ocean temperature changes from Argo (contour interval is 0.01 °C for colours, 0.05 °C in grey); (c) Global ocean 0–2 000 m heat content change over time; (d) Global average 2006–November 2015 potential temperature trend (°C per decade) plotted against depth; and (e) Heat content trends plotted against latitude. Plots (c), (d) and (e) show results for three Argo-based analyses: OI (red), RSOI (blue) and RPF (dotted), which provide indication of uncertainty. *(Source: Reproduced from Wijffels et al. (2016), where full details are available.)*

For more information, please contact:

World Meteorological Organization

7 bis, avenue de la Paix – P.O. Box 2300 – CH 1211 Geneva 2 – Switzerland

Communication and Public Affairs Office

Tel.: +41 (0) 22 730 83 14/15 – Fax: +41 (0) 22 730 80 27

E-mail: cpa@wmo.int

www.wmo.int

JN 16227